INTL JOURNAL OF ELECTRONICS AND TELECOMMUNICATIONS, 2024, VOL. 70, NO. 4, PP. 805-813
Manuscript received August 24, 2024; revised October 2024. doi: 10.24425/ijet.2024.152064

Shallow water communication with an object buried in bottom sediments

Roman Salamon, Jacek Marszal, and Iwona Kochańska

***Abstract*—Underwater acoustic communications (UAC) in shallow water applications is a very difficult task. This task becomes even more difficult when there is a need to ensure reliable communication with an object buried in bottom sediments. The article presents a simulation of an acoustic transmission channel in conditions of strong multi-path propagation to an object buried in bottom sediments. The impulse response method was used, supported by a technique derived from the ray tracing image source method. Simulation results are presented for both narrowband and broadband signals with LFM frequency modulation. Based on the simulation, the conditions that should be met by the transmission signals to ensure correct communication were determined. Examples of data transmission to an object buried in bottom sediments in a simulated shallow channel with multi-path propagation were also presented.**

***Keywords*—underwater acoustic communications; UAC; shallow water channel; multipath propagation; bottom sediments**

I. Introduction

FOR OVER 20 YEARS, the Faculty of Electronics, Telecommunications and Informatics of the Gdańsk University of Technology has been conducting research and development work related to underwater acoustic communication in shallow waters [1-10]. While conducting experiments related to the above work, the problem of establishing communication with an object buried in soft bottom sediments often arose. In the research on this topic currently carried out at the Gdańsk University of Technology, one of the main goals of research is to ensure reliable communication with an object buried in bottom sediments.

Topics related to the propagation of acoustic waves in bottom sediments are the subject of numerous works published from the 1960s to the present. Here are a selection of them - [11-20]. The above works mainly present the results of in-situ measurements of attenuation coefficients and speeds of acoustic waves in various bottom sediments, as well as theoretical analyses of propagation conditions in these media. There are also numerous works in which models describing the propagation of acoustic waves in shallow waters are proposed [21-24].

The following chapters present a slightly different approach to describing the propagation of acoustic waves in shallow water. The created model also takes into account the issue of obtaining communication with an object buried in bottom sediments. The aim of this approach is to describe the properties of the channel by determining its impulse response. This will enable the calculation of its transfer function and the analysis of transmission properties for digital data transmission using various types of modulation and coding.

II. Assumptions

A simplified model of an acoustic wave communication system in a water channel bounded by a flat water surface and a flat bottom parallel to this surface will be considered. In the system, there is a direct wave spreading from a source submerged in the water to an object in the water and to an object buried in the bottom sediments. In addition to the direct wave, there are reflected waves from both boundary surfaces. The reflection and transmission of the wave into the bottom sediments will be described with a spherical-wave reflection model, taking into account the characteristic acoustic impedance of the air, water and bottom sediments and the angle incidence of the wave. Absorption attenuation in water and bottom sediments will be taken into account. The method used here to determine the impulse response, is similar to the image source method used to determine the impulse response of rooms [25-27]. Assuming a linear wave propagation model, we will describe the system model by the impulse response that is the response of the receiver to the Dirac impulse emitted by the wave source. The signal received at the object will therefore be a convolution of the impulse response and the signal generated by the source.

III. System Model with an Object Submerged in Water

Let us first consider the signals reflected first from the surface of the water. Their path is illustrated in Fig.1. It results from the figure above that the direct wave path from the source to the object is equal to:

$$r_o = \sqrt{x^2 + (h - d - w)^2} \tag{1}$$

With the odd number of reflections shown in the left figure, we have $x = a + (n-1)b + e$, where n is the number of reflections.

Since $a = h \cdot \tan\alpha$, $b = d \cdot \tan\alpha$ and $e = (d - w) \cdot \tan\alpha(n)$, the distance x of the object from the source calculated over the water surface is equal to:

The paper was written as a result of the research project No. DOB-SZAFIR/01/B/017/04/2021 financed by The National Centre for Research and Development of the Republic of Poland.

Authors are from Gdansk University of Technology, Faculty of Electronics, Telecommunications and Informatics, Department of Signals and Systems, Gdańsk, Poland. (e-mail: {roman.salamon, jacek.marszal, iwona.kochanska}@pg.edu.pl).

$$x = (nd + h - w)\tan\alpha(n) \quad (2)$$

where $\alpha(n)$ is the angle of incidence of the wave at n reflections.

With an even number of reflections, we have $e = w\cdot\tan\alpha(n)$, thus:

$$x = [(n-1)d + h + w]\tan\alpha(n) \quad (3)$$

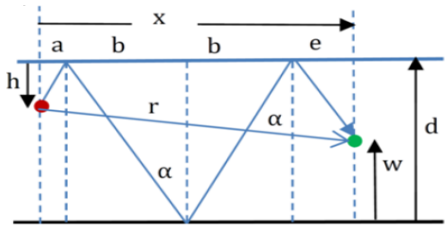

Fig. 1a. Paths of the wave first reflected from the water surface; odd number of reflections.

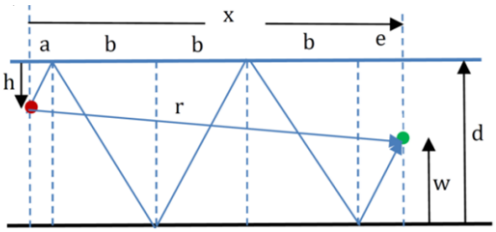

Fig. 1b. Paths of the wave first reflected from the water surface; even number of reflections.

The path of the wave at n reflections is equal to $r = [a + (n-1)b + e]\cdot\sin\alpha(n)$, and hence we obtain at an odd number of reflections:

$$r(n) = (nd + h - w)/\cos\alpha(n) \quad (4)$$

and with an even number of reflections:

$$r(n) = [(n-1)d + h + w]/\cos\alpha(n) \quad (5)$$

Hence the path length $r(n)$ of the reflected waves equals:

$$r(n) = \frac{x}{\sin\alpha(n)} \quad (6)$$

The calculation procedure is to determine the angle $\alpha(n)$ from formulas (2) and (3) and to determine the path $r(n)$ from the formula (6). Knowing the r_o and $r(n)$ distances, we calculate the wave lags from the formulas:

$$\tau_o(n) = \frac{r_o}{c} \qquad \tau(n) = \frac{r(n)}{c} \quad (7)$$

where c is the speed of the acoustic wave in water.

The value of the pressure p_o of the direct signal received by the object can be derived from the formula:

$$p_o = p_1\frac{r_1}{r_o}10^{\alpha_w r_o/20} \quad (8)$$

where p_1 is the pressure of the signal emitted by the source at r_1 distance from it, and α_w is the water absorption attenuation ratio [dB/m].

The value of the acoustic pressure of the reflected signals received by the object is:

$$p(n) = p_1\frac{r_1}{r(n)}R_w(n)\cdot R_d(n)\cdot 10^{\alpha_w r(n)/20} \quad (9)$$

where $R_w(n)$ is the total reflection ratio from the water surface and $R_d(n)$ is the total reflection ratio from the bottom surface.

The single reflection coefficient at the water-sediments boundary is used in the formula:

$$R_{d1}(n) = \frac{z_d\cdot\cos\alpha(n) - z\cdot\cos\beta(n)}{z_d\cdot\cos\alpha(n) + z\cdot\cos\beta(n)} \quad (10)$$

where $z_d = \rho_d c_d$, (ρ_d is the volume density of the bottom sediments, c_d is the acoustic wave speed in the bottom sediments) and $z = \rho c$ is the corresponding volumes for water.

The β angle is the angle of refraction derived from Snell's law:

$$\frac{c}{c_d} = \frac{\sin\alpha}{\sin\beta} \quad (11)$$

The total reflection ratio takes into account multiple reflections from the bottom surface and is:

$$R_d(n) = [R_{d1}(n)]^m \quad (12)$$

where m is the number of reflections from the bottom surface and $m = \frac{(n-1)}{2}$ when n is an odd number and $m = \frac{n}{2}$ when n is an even number.

Due to the much higher characteristic acoustic impedance of water than air, we assume that $R_{w1}(n) = -1$, and then:

$$R_w(n) = [-1]^p \quad (13)$$

where for n odd numbers, $p=(n+1)/2$ and for m even numbers, $p=n/2$. In calculations where we consider wave dispersion on boundary surfaces, we multiply the single reflection ratios $R_{d1}(n)$ and $R_{w1}(n)$ by the assumed dispersion ratios.

The wave paths at the first reflection from the bottom surface are shown in Fig. 2a and Fig. 2b.

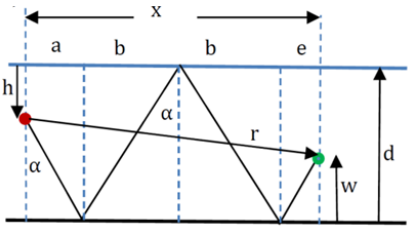

Fig. 2a. Path of the wave first reflected from the bottom surface; odd number of reflections.

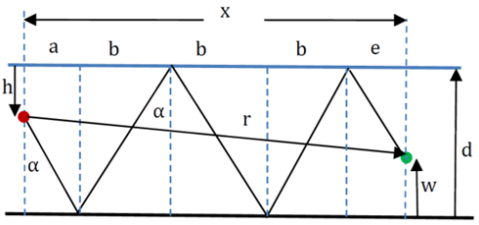

Fig. 2b. Path of the wave first reflected from the bottom surface; even number of reflections.

The following dependencies now occur:

- for an even number of n reflections

$$x = [(n+1)d + w + h]\,tan\,\alpha(n) \quad (14)$$

$$r(n) = [(n+1)d - (h+w)]/\cos\alpha(n) \quad (15)$$

- for an odd number of n reflections

$$x = [nd + w - h]\,tan\,\alpha(n) \quad (16)$$

$$r(n) = [nd + w - h]/\cos\alpha(n) \qquad (17)$$

As before, after determining the $\alpha(n)$ angles from formulas (14) and (16), the $r(n)$ lengths of the wave paths from formula (6) and the $\tau(n)$ delay from formula (7) the pressure of the wave received by the object is calculated from formulas (9) to (13) with $m=(n+1)/2$ for an odd n and $m=n/2$ for an even n inserted into formula (12). In formula (13), we insert $p=(n-1)/2$ for an odd n and $p=n/2$ for an even n.

Fig. 3 shows an example impulse response for an object distance of x=50 m and Fig.4 for a distance of x=200 m.

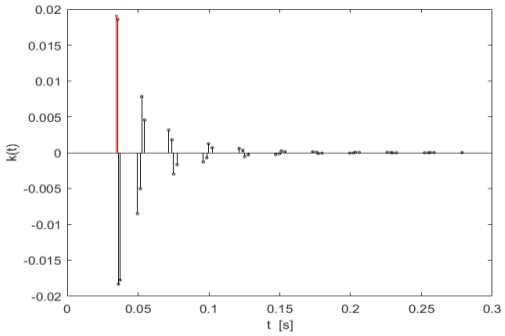

Fig. 3. Impulse response for the object immerse in water x=50m, (h=3m, w=2m, c=1500m/s, c_d=1800m/s, ρ=1000kg/m^3, ρ_d=3000kg/m^3, α=0.001dB/m)

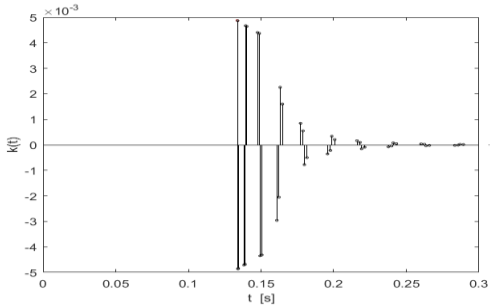

Fig. 4. Impulse response for the object immerse in water x=200m, (other parameters as in Fig. 3)

With an increasing object distance, a deterioration in the relationship between the magnitude of the direct signal and the magnitude of the reflected signals is apparent.

The following figures show parts of the transfer function module determined from Fourier transform: $K(f) = \mathcal{F}\{k(t)\}$.

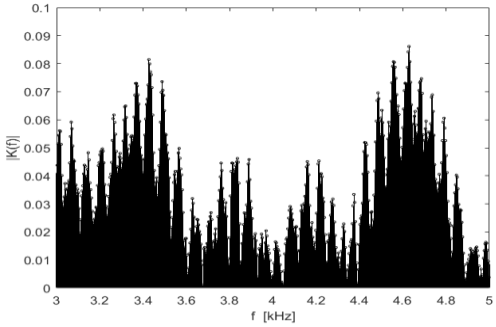

Fig. 5. Transfer function for impulse response from Fig. 3.

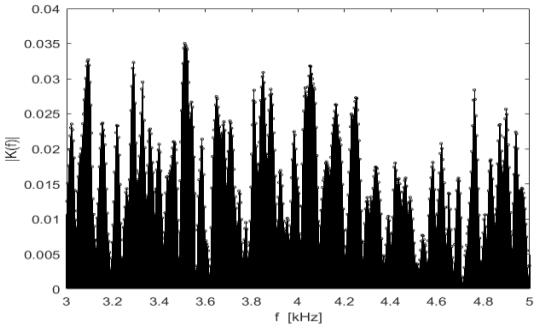

Fig. 6. Transfer function for impulse response from Fig. 4

Both transfer functions have a quasi-periodic waveform with very large differences between local maxima and minima. The general conclusion is that the transmission of narrowband signals depends very strongly on the choice of carrier frequency. In the absence of a priori knowledge of the transfer function, a communication system using narrowband signals has uncontrolled parameters (mainly range) and should be considered practically useless. Some improvement can be expected from the use of signals with a wider spectrum.

IV. SYSTEM MODEL WITH AN OBJECT SUBMERGED IN WATER

The direct wave path from the source to the object buried in the bottom sediments is illustrated in Fig. 7.

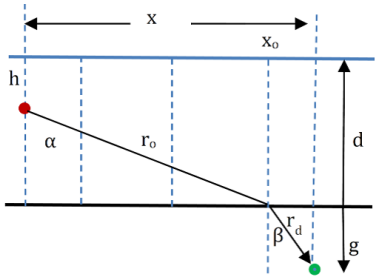

Fig. 7. Direct wave path to the object buried in the bottom sediments

The following dependencies emerge from the geometry shown above:

$$r_o = \sqrt{x_o^2 + (d-h)^2} \qquad (18)$$

$$r_d = \sqrt{(x-x_o)^2 + g^2} \qquad (19)$$

$$\sin\alpha = \frac{x_o}{r_o} \qquad (20)$$

$$\sin\beta = \frac{x - x_o}{r_d} \qquad (21)$$

From Snell's law, we have:

$$\frac{\sin\alpha}{\sin\beta} = \frac{c}{c_d} \qquad (22)$$

where c is the acoustic wave speed in water, and c_d is the speed in the bottom sediments.

By inserting the (20) and (21) dependencies into the above formula, we obtain:

$$\frac{c}{c_d} = \frac{x_o \cdot r_d}{(x - x_o)\cdot r_o} \qquad (23)$$

and from equations (18) and (19), when equation (23) is squared, we have:

$$\left(\frac{c}{c_d}\right)^2 - \frac{x_o^2 \cdot [(x-x_o)^2 + g^2]}{(x-x_o)^2 \cdot [x_o^2 + (d-h)^2]} = 0 \qquad (24)$$

This is an equation of the fourth degree with respect to x_o, which can be solved numerically. The determined xo distance is inserted into the dependencies in (18) and (19), and from these, the wave path from the source to the object $r=r_o+r_d$ and the delay are calculated:

$$\tau = \frac{r_o}{c} + \frac{r_d}{c_d} \qquad (25)$$

The pressure of the acoustic wave received by the object is:

$$p = p_1 T \frac{r_1}{r} 10^{(a_w r_o + a_d r_d)/20} \qquad (26)$$

where αd means the absorption attenuation ratio of the bottom sediments.

The T symbol is the wave transmission ratio at the water-bottom sediments interface and is represented by the formula:

$$T = \frac{2z_d \cdot \cos\alpha}{z \cdot \cos\beta + z_d \cdot \cos a} \qquad (27)$$

where $z=\rho c$ is the characteristic impedance of the water and $z_d=\rho_d c_d$ of the bottom sediments, (ρ and ρ_d are the volume densities of the water and sediment, and c and c_d are the acoustic wave speed in the water and bottom sediments, respectively). α and β angles are derived using formulas (20) and (21).

The routes of the waves first reflected from the water surface and passing into the bottom sediments are illustrated by Fig. 8a, and first reflected from the bottom surface – Fig. 8b.

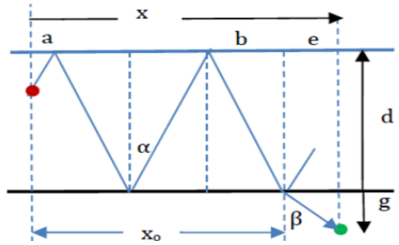

Fig. 8a. Paths of waves reflected from the source to the object buried in the bottom sediments - first reflected from the water surface

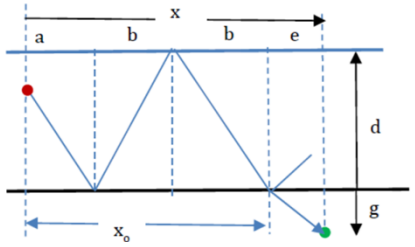

Fig. 8b. Paths of waves reflected from the source to the object buried in the bottom sediments - first reflected from the bottom surface

Let us first consider the path of the wave first reflected from the water surface. It follows from Fig. 8a that

$$x_0 = a + nb \qquad x - x_0 = e \qquad (28)$$

where n is the number of reflections from the water and the bottom surface (in the figure, n=3) and

$$a = h\tan\alpha(n), b = d\tan\alpha(n), e = g \cdot \tan\beta(n) \qquad (29)$$

After putting the dependencies from (29) into formula (28), we obtain:

$$x_0(n) = (h + nd)\tan\alpha(n), \quad x - x_0(n) = g\tan\beta(n) \qquad (30)$$

The length of the path from this source to the refraction point is equal to:

$$r_w(n) = \sqrt{(h+nd)^2 + x_0^2(n)} \qquad (31)$$

and the r_d distance is:

$$r_d(n) = \sqrt{[x - x_0(n)]^2 + g^2} \qquad (32)$$

As we have:

$$\sin\alpha(n) = \frac{r_w(n)}{x_0(n)}, \qquad \sin\beta(n) = \frac{r_d(n)}{x - x_0(n)} \qquad (33)$$

so it follows from Snell's law that

$$\frac{c}{c_d} = \frac{\sin\alpha(n)}{\sin\beta(n)} = \frac{x \cdot r_w(n)}{[x - x_0(n)]x_0} \qquad (34)$$

After applying the dependencies from (31) and (32), we get:

$$\frac{c}{c_d} - \frac{x \cdot \sqrt{(h+nd)^2 + x_0^2(n)}}{x_0(n)\sqrt{[x - x_0(n)]^2 + g^2}} = 0 \qquad (35)$$

This is a fourth-degree equation with respect to x_0, which can be solved numerically for successive n reflections from the water surface. It can be seen from Fig. 8a. that only odd reflections should be considered.

After determining the x_0 distance, we calculate the rw distance from formula (31) and the r_d distance from formula (32) and from there we calculate the delay of the signal received by the object relative to when the signal is sent by the sound source. The delay is:

$$\tau(n) = \frac{r_w}{c} + \frac{r_d}{c_d} \qquad (36)$$

The acoustic pressure of the wave received by the submerged object is expressed by the formula:

$$p_w(n) = p_1(-1)^p T(n)[R_d(n)]^m \frac{r_1}{r_h + r} 10^{(a_w r_n + a_d r_0)/20} \qquad (37)$$

where $R_d(n)$ is described by formula (10), $T(n)$ by formula (27) and $p=(n+1)/2$, $m=(n-1)/2$, for an odd n only. The $\alpha(n)$ and $\beta(n)$ angles are calculated from formula (33) after determining the x_0 distance.

In the case of the first reflection first from the bottom surface illustrated in Fig. 8b, the following dependencies occur:

$$x_0 = a + (n-1)b \qquad x - x_0 = e \qquad (38)$$

and

$$a = (d-h)\tan\alpha(n), \; b = d\tan\alpha(n), \quad e = g\tan\beta(n) \qquad (39)$$

After putting the dependencies in (39) into formula (38) we receive:

$$x_0(n) = (h + nd)\tan\alpha(n), \; x - x_0(n) = g\tan\beta(n) \qquad (40)$$

The length of the path from this source to the refraction point is equal to:

$$r_w(n) = \sqrt{(nd-h)^2 + x_0^2(n)} \tag{41}$$

and the r_d distance is:

$$r_d(n) = \sqrt{[x - x_0(n)]^2 + g^2} \tag{42}$$

After putting the above-mentioned dependencies into formulas (33) and (34), we obtain

$$\frac{c}{c_d} - \frac{x \cdot \sqrt{(nd-h)^2 + x_0^2(n)}}{x_0(n)\sqrt{[x - x_0(n)]^2 + g^2}} = 0 \tag{43}$$

After solving the above equation relative to x_0, we determine the $\tau(n)$ delay from formula (36) and the $p_w(n)$ pressure from formula (37). Formula (37) is now only valid for an even number of n reflections, and p=m=n/2.

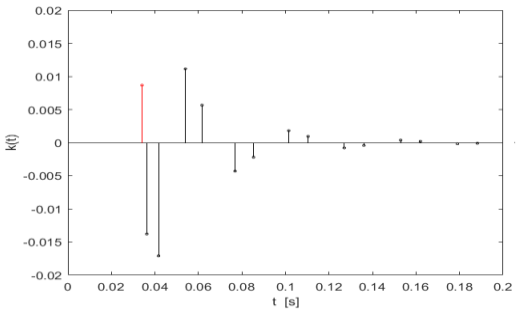

Fig. 9. Impulse response for the object buried in bottom sediments (x=50 m)

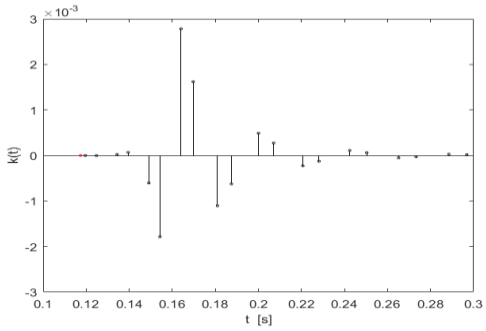

Fig. 10. Impulse response for the object buried in bottom sediments (x=200 m)

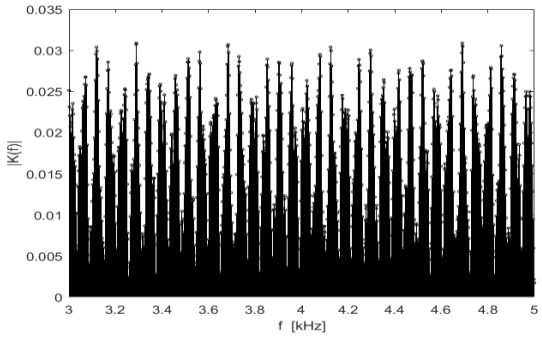

Fig. 11. Transfer function for the object buried in bottom sediments (x=50 m)

The Figures 9-12 show examples of impulse responses and transfer functions for the object buried in the water. The parameters given in the caption of Fig. 3 were retained and the burial depth g=1 m and the absorption attenuation ratio in the bottom sediments α_d=0.5 dB/m were assumed. The transfer function seen in Fig. 11 is derived from the impulse response shown in Fig. 9. Similarly, Fig. 12 corresponds to Fig. 10.

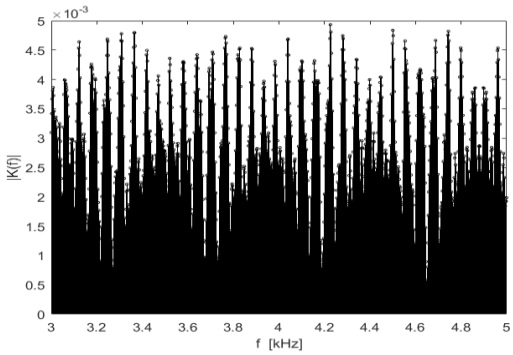

Fig. 12. Transfer function for the object buried in bottom sediments (x=200 m)

With a small distance x=50 m, the impulse response waveform is similar to the impulse response for the object immersed in water. There is only a slight deterioration in the relationship between direct and reflected signals. This deterioration increases significantly with the increasing object distance from the sound source, as illustrated in Fig. 10. This is due to the increase in the distance the wave travels in the bottom sediments, where the absorption attenuation is much greater than the attenuation in the water. In the examples shown in the figures, for the object 50 m away, the bottom sediments wave path is 24.4 m, and for the object 200 m away, it is equal to 174.4 m. In the first case, the attenuation loss is 12.2 dB and in the second case 87.2 dB. The direct signal received by the object at x=200 m is 5600 times smaller than the signal received from 50 m (ignoring spreading losses). This leads to the general conclusion that signal transmission at longer distances takes place almost exclusively on reflected waves.

Similarly, as in Fig. 5 and Fig. 6, the transfer functions shown in Fig. 11 and Fig. 12 have a quasi-periodic waveform, prompting the use of broad-spectrum signals.

Impulse responses can be characterised by several parameters, namely: the τ_0 time, which elapses from the emission of the signal to the reception of the first impulse, the τ_{max} time, calculated from the emission of the signal to the reception of the maximum impulse, and the τmin time, measured from the emission of the signal to the reception of an impulse 40 dB smaller than the maximum impulse. We define the δ_τ=τ_{min} - τ_{max} time difference as the duration of the impulse response. The dependencies of these parameters on the object's x distance are shown in Fig. 13 and Fig. 14. Fig. 13 refers to the object buried in the bottom sediments at a depth of g=2 m, and Fig. 14 refers to the object in the depths above the bottom surface with a height of w=2 m.

It can be seen from both figures that the duration of the impulse response only slightly depends on the distance of the object. Fig. 14 shows that for longer distances, the largest impulse is received later than the direct impulse, as shown in Fig. 10. For the object immersed in water above the bottom surface, the direct impulse is always the largest.

The dependence of the magnitude of the maximum impulse response on the object distance is shown in Fig.15 and Fig.16, with the object burial depth increased to g=5m and the height above the bottom surface to w=5m in Fig.16. It can be seen from the figures that, for greater distances, the impulse response for objects submerged in water is greater than that from objects buried in the bottom sediments and increases with depth of immersion.

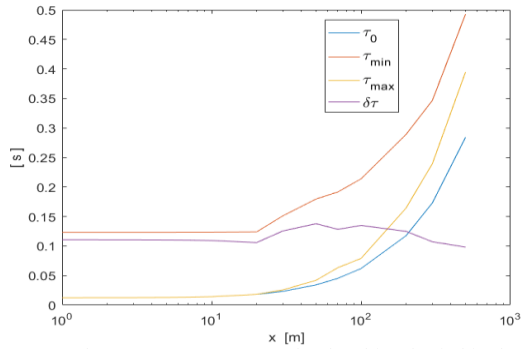

Fig. 13. Impulse response parameters for the object buried in the bottom sediments

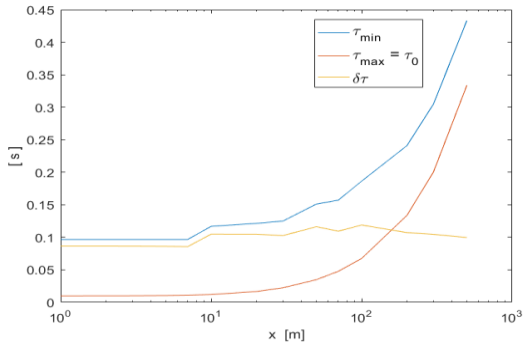

Fig. 14. Impulse response parameters for the object immersed in water

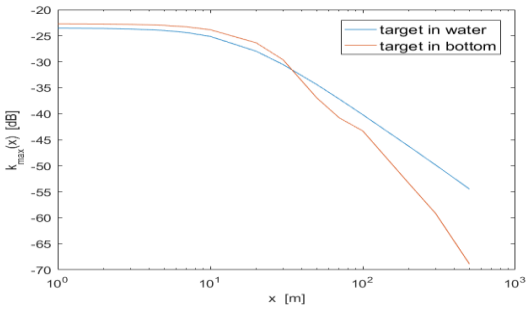

Fig. 15. Dependence of the maximum volume of the impulse response on the object distance

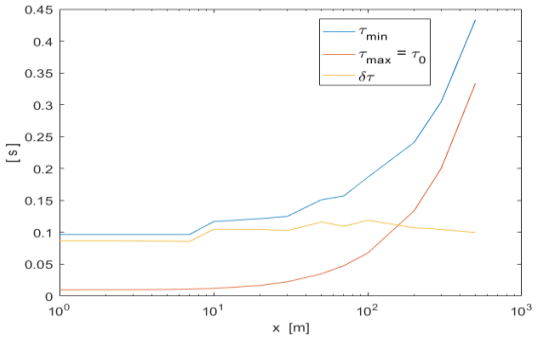

Fig. 16. Dependence of the maximum volume of the impulse response on the object distance

The calculations performed showed, which for lack of space we do not cite here, that changing the parameters of the medium and the system influences the impulse response waveform, but does not change the trends described above.

V. TRANSMISSION OF SIGNALS IN THE SYSTEM

Knowing the impulse response of the system $k(t)$, it is possible to determine the $y(t)$ signals at the output of the receiver installed at the object for any $s(t)$ signals emitted by the transmitters, using convolution function:

$$y(t) = \int_0^t s(\tau)k(t-\tau)d\tau \qquad (44)$$

We assume that short digital information will be sent through the system. We will consider two signals that enable such transmission, namely a sequence of sinusoidal pulses and a sequence of linear frequency modulation (LFM) pulses. In the first case, the bits will be distinguishable by the carrier frequency. Fig. 17 and Fig. 18 show the envelopes of received signals consisting of two following each other sinusoidal pulses of τ_i=100 ms duration and frequencies of f_0=4 kHz (red colour) and f_1=3.5 kHz (black colour). The pulse interval is 100 ms. In Fig. 17, the object distance is x=50 m and in Fig. 18, the distance is x=200 m. The system parameters are given in the caption of Fig. 3. This figure and Fig. 4 show the impulse responses used to determine the signals analysed here. Envelope detection consists of full-wave rectification and low-band filtering with a Butterworth filter with a bandwidth of 100 Hz. The proportions between the bit signals amplitude in the figures are inverted as a result of the different transfer function waveforms shown in Fig. 5 and Fig. 6.

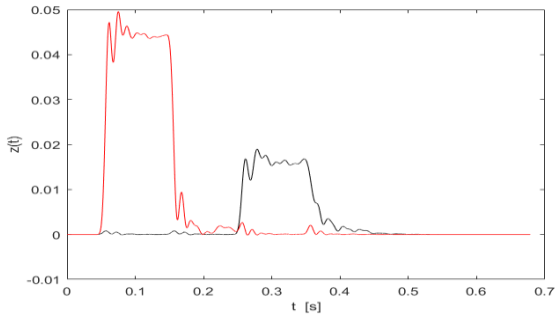

Fig. 17. The envelopes of received signals consisting of two sinusoidal pulses of τ_i=10ms duration and frequencies of f_0=4kHz (red) and f_1=3.5kHz (black). Distance x=50m

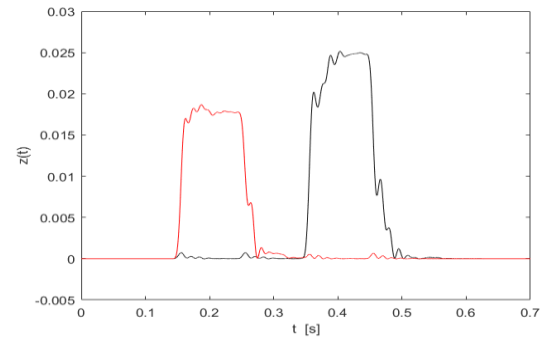

Fig. 18. The envelopes of received signals as in Fig. 17, for distance x=200m

The analogous signals for the buried object are shown in Fig. 19 and Fig. 20. The corresponding impulse responses to which the figures refer are shown in Fig. 9 and Fig. 10.

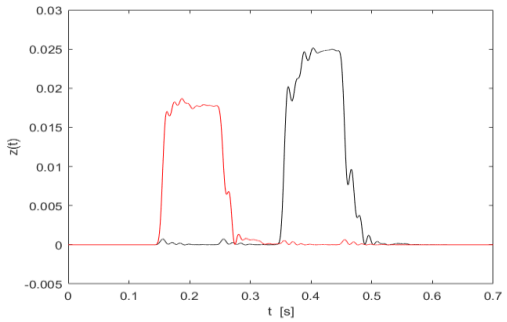

Fig. 19. Envelopes of signals received by the object buried in the bottom sediments (parameters as in Fig. 17), x=50m

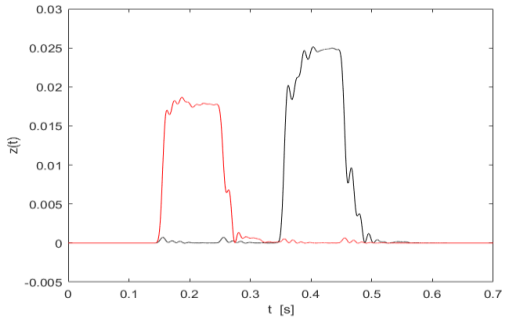

Fig. 20. Envelopes of signals received by the object buried in the bottom sediments (parameters as in Fig. 17), x=200m

Comparing the figures produced for the object submerged in water to those for the object buried in the bottom sediments, we notice a decrease in the magnitude of the signals reaching the buried object. This effect is greater for greater object distance, as the ratio is as 1:0.15. This is due to the longer propagation path of the wave in the bottom sediments, where there is greater absorption attenuation.

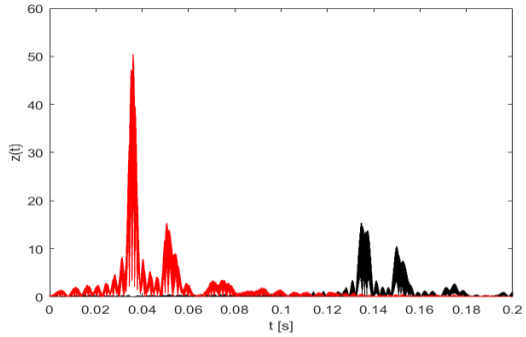

Fig. 21. LFM signals received by the object submerged in water (x=50 m)

The benefits of using LFM signals are illustrated in the Figures 21-24. The calculations were performed for a pair of LFM impulses with carrier frequencies of 3.5 kHz and 4 kHz and a bandwidth of 400 Hz. The duration of the impulses is 0.1 s and they are transmitted without interruption. Matched filtering is realised in the receiver, described by the following dependence:

$$z(t) = \mathcal{F}^{-1}[\mathcal{F}\{s(t)\} \cdot \mathcal{F}^{*}\{y(t)\}] \tag{45}$$

where the symbol $\mathcal{F}\{\ \}$ indicates the Fourier transform, $s(t)$ describes the transmitted signal, and $y(t)$ the received signal.

In Fig. 21 and Fig. 22, the output signals come from the object submerged in the water, and in Fig. 23 and Fig. 24 from the object buried in the bottom sediments. The impulse responses are the same as those relating to the previous figures.

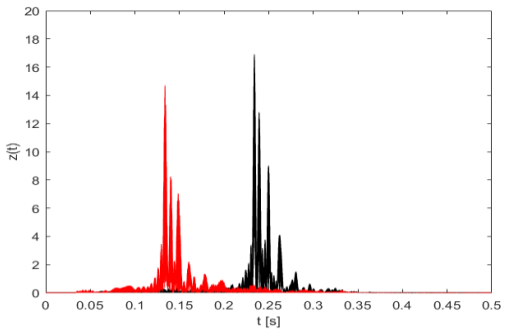

Fig. 22. LFM signals received by the object submerged in water (x=200m).

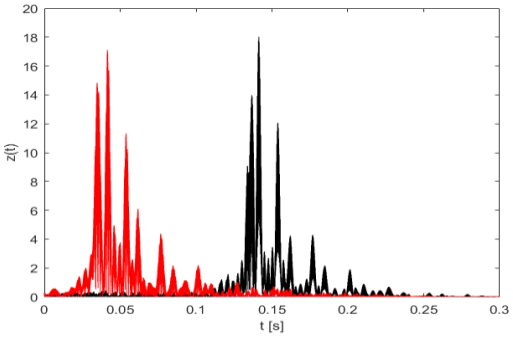

Fig. 23. LFM signals received by the object buried in the bottom sediments (x=50m)

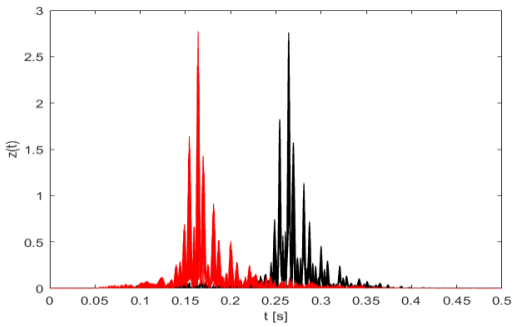

Fig. 24. LFM signals received by the object buried in the bottom sediments (x=200m)

The figures show the change in shape of the LFM signals in relation to the sinusoidal impulses. The shapes are close to the corresponding impulse responses. In line with the properties of matched filtering, the magnitude of these signals also increased many times. Both the shape and magnitude of the signals improve the detection conditions, as we will demonstrate by analysing the noise in the system.

We will describe the effect of noise on detection in the analysed system by the input and output signal-to-noise ratio. The input signal-to-noise ratio is described by the dependency:

$$SNR_i = 20\log\frac{y_{max}}{\sigma} \tag{46}$$

where y_{max} is the maximum value of the signal at the receiver's input and σ is the rms value of the noise at the receiver's input in its B bandwidth. In the simulation calculations, Gaussian noise of σ_o was generated and converted using the formula:

$$\sigma = \sigma_o \sqrt{\frac{2B}{f_s}} \tag{47}$$

where f_s is the sampling rate.

For sinusoidal impulses, the B-band width is the bandwidth of the filters in the receiver, while for LFM signals, it is equal to the bandwidth of the transmitted signal.

The analogous formula describes the output signal-to-noise ratio SNR_o, where y_{max} is the maximum signal value and σ is the rms of the noise at the receiver input.

Fig. 25 shows the noisy signal from Fig. 17 (object in water) and Fig. 26 shows the noisy signal from Fig. 19 (object buried in the bottom sediments). Both figures refer to sinusoidal impulses and the object distance of x=50 m.

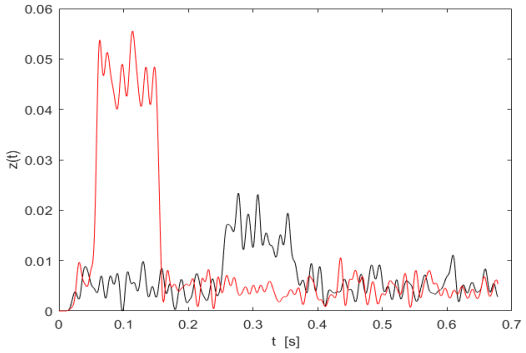

Fig. 25. Noisy signals received by the object immersed in water

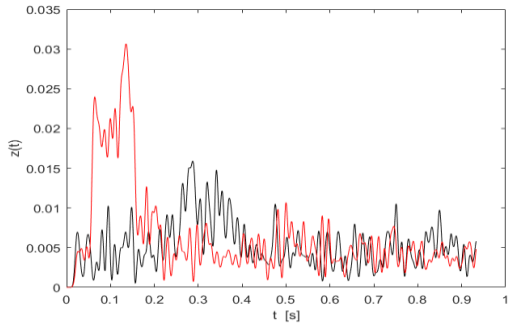

Fig. 26. Noisy signals received by the object buried in the bottom sediments

Signal-to-noise ratios differ for the bit signals and so for the first signal reaching the object in the water, we have SNR_i=25.4dB and SNR_o=27.4 dB, and for the second impulse, SNR_i=17.5 dB and SNR_o=18dB. The improvement in the signal-to-noise ratio in the first case is 2 dB and 1.4 dB in the second. For the object buried in the bottom sediments, for the first impulse, we have SNR_i=19.2 dB and SNR_o=22.5 dB, and for the second impulse, SNR_i=15.3 dB and SNR_o=17.3 dB. The improvements in the signal-to-noise ratio are 3.2 dB and 2 dB, respectively.

As it is known, the application of the LFM signal results in an improvement of the output signal-to-noise ratio compared to the input signal-to-noise ratio. This improvement is proportional to the product of the B bandwidth and the τ_i. impulse duration. This is illustrated in the following figures produced for τ_i=1 s. In the system considered here, there are virtually no constraints on the information transmission time and the overriding requirement is to ensure minimum errors.

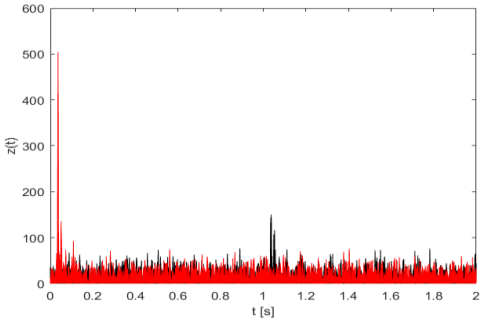

Fig. 27. Noisy output LFM signals from the object submerged in water

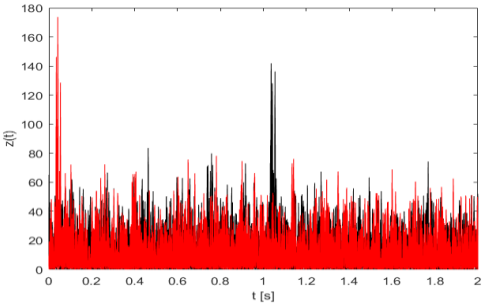

Fig. 28. Noisy output LFM signals from the object buried in the bottom sediments

In the situation shown in Fig. 27, the signal-to-noise ratios for the first impulse are SNR_i=7.4dB and SNR_o=32.0 dB, and for the second impulse, SNR_i=0.4 dB and SNR_o=22.3dB. The improvement in the signal-to-noise ratio in the first case is 24.6 dB and 21.9 dB in the second. By comparing these results with the one obtained for the signal in Fig. 25, we see a significant improvement in the signal-to-noise ratios discussed. These are lower than those obtained with full matching of the output signal to the input signal, which is 29 dB. This is due to the impulse response of the system, which differs from the theoretical response $k(t)=\delta(t-\tau)$.

For the object buried (Fig. 28) in the bottom sediments, for the first impulse, we have SNR_i=3.0 dB and SNR_o=23.1 dB, and for the second impulse, $SNRi$=1.3 dB and SNR_o=22.9 dB. The improvements in the signal-to-noise ratio are 20.1 dB and 21.6 dB, respectively. There is a noticeable deterioration in the output signal-to-noise ratio in relation to the object in water despite the assumed equal spectral density of noise power.

CONCLUSIONS

It is shown that the impulse response method used is a convenient tool for analysing the transmission of acoustic signals between a transmitter and objects submerged in water and buried in the bottom sediments. The calculations presented show a large difference between the magnitude of the impulse response for the object submerged in water and the object buried in the bottom sediments, which is the result of the much greater absorption attenuation in the sediment compared to that in water. The analysis carried out on the influence of channel parameters on impulse responses showed the main effect of the object's distance from the sound source on their magnitude, resulting in the transmission system's range being limited to single hundreds of metres. In the case of objects buried in the bottom sediments, the extent of absorption attenuation in the

bottom sediments has a strong influence on the system's range. The channel parameters have no significant effect on the duration of the impulse response, which translates into the rate of information transmission. An interesting observation is that, at longer ranges, transmission with the object buried in the bottom sediments takes place on reflected waves rather than direct waves. To sum up, it should be emphasized, that:

- Correct shallow water data transmission to an object buried in bottom sediments is possible.
- The smaller the range, the greater the chance of correct transmission;
- The probability of correct transmission decreases with the depth of burial of the object and with the increase of the sediments acoustic impedance;
- Better conditions for correct transmission are provided by signals with linear frequency modulation with matched filtering;
- To improve detection conditions, wideband LFM pulse trains of long time duration as possible should be used.

REFERENCES

[1] K. Zachariasz, J. Schmidt, R. Salamon., "Code signals transmission using MFSK modulation in shallow waters", *Hydroacoustics*, Vol.4, pp. 261-264, 2001.

[2] J. Schmidt, K. Zachariasz, R. Salamon., "Underwater communication system for shallow water using modified MFSK modulation", *Hydroacoustics*, vol. 8, pp. 179-184, 2005.

[3] J. Schmidt., "Reliable underwater communication system for shallow coastal waters", *Hydroacoustics*, vol. 17, pp. 171-178, 2014.

[4] J. Schmidt, I. Kochańska, A. Schmidt, "Measurement of impulse response of shallow water communication channel by correlation method", *Hydroacoustics*, vol. 20, pp. 149-158, 2017.

[5] I. Kochańska, J. H. Schmidt, J. Marszal, "Shallow water experiment of OFDM underwater acoustic communications", *Archives of Acoustics*, vol. 45, no. 1, 11-18, 2020, https://doi.org/10.24425/aoa.2019.129737

[6] I. Kochańska, "Reliable OFDM Data Transmission with Pilot Tones and Error-Correction Coding in Shallow Underwater Acoustic Channel", *Applied Sciences*, vol. 10, no. 6, pp. 2173, 2020. https://doi.org/10.3390/app10062173

[7] I. Kochańska, "A new direct-sequence spread spectrum signal detection method for underwater acoustic communications in shallow-water channel", *Vibrations in Physical Systems*, vol. 32, no. 1, pp. 2021106, 2021. https://doi.org/10.21008/j.0860-6897.2021.1.06

[8] I. Kochańska, "Erratum: A new direct-sequence spread spectrum signal detection method for underwater acoustic communications in shallow-water channel", *Vibrations in Physical Systems*, vol. 33, no. 1, pp. 2022114, 2022. https://doi.org/10.21008/j.0860-6897.2022.1.14

[9] J. Schmidt, A. Schmidt., "Synchronization system for underwater acoustic communications using in shallow waters", *Vibrations in Physical Systems*, vol. 34, no. 1, pp. 2023102, 2023, https://doi.org/10.21008/j.0860-6897.2023.1.02

[10] J. H. Schmidt, A. M. Schmidt, "Wake-up receiver for underwater acoustic communication using in shallow water", *Sensors*, vol. 23, no. 4, 2088, 2023, https://doi.org/10.3390/s23042088

[11] A. B. Wood, D. E. Weston, "The propagation of sound in mud, *Acustica*, vol. 14, pp. 156 - 162,1964.

[12] R. D. Stoll, G. M. Bryan, "Wave Attenuation in Saturated Sediments", *J. Acoust. Soc. Am.*, vol. 47, no. 5, part 2, pp. 1440-1447, 1970. https://doi.org/10.1121/1.1912054

[13] R. D. Stoll, "Theoretical aspects of sound transmission in sediments", *J. Acoust. Soc. Am.*, vol. 68, no. 5, pp. 1341-1350, 1980. https://doi.org/10.1121/1.385101

[14] R. D. Stoll, "Marine sediment acoustics", *J. Acoust. Soc. Am.*, vol. 77, no. 5, pp. 1789-1799, 1985. https://doi.org/10.1121/1.391928

[15] A. C. Kibblewhite, "Attenuation of sound in marine sediments: A review with emphasis on new low-frequency data", *J. Acoust. Soc. Am.*, vol. 86, no. 2, pp. 716-738, 1989. https://doi.org/10.1121/1.398195

[16] M. J. Buckingham, "Theory of acoustic attenuation, dispersion, and pulse propagation in unconsolidated granual materials including marine sediments", *J. Acoust. Soc. Am.*, vol.102, no. 5, pp. 2579-2596, 1997. https://doi.org/10.1121/1.420313

[17] A. Turgut, T. Yamamoto, "In Situ measurements of velocity dispersion and attenuation in New Jersey Shelf sediments", *J. Acoust. Soc. Am.*, vol. 124, no.3, pp. EL122-EL127, 2008. https://doi.org/10.1121/1.2961404

[18] K. M. Lee, M. S. Ballard, A. R. McNeese, T. G. Muir, P. S. Wilson, "In situ measurements of sediment acoustic properties in Currituck Sound and comparison models", *J. Acoust. Soc. Am.*, vol. 140, no. 5, pp. 3593-3606, 2016. https://doi.org/10.1121/1.4966118

[19] M. S. Ballard, "The acoustics of marine sediments", *Acoustics Today*, vol. 13, no. 3, pp. 11-18, 2017.

[20] C. W. Holland, S. E. Dosso, "On compressional wave attenuation in muddy marine sediments", *J. Acoust. Soc. Am.*, vol. 149, no. 5, pp. 3674-3687. https://doi.org/10.1121/10.0005003

[21] M. Stojanovic, J. Preisig, "Underwater acoustic communication channels: prpagation models and statistical characterisation", *IEEE Communications Magazine*, January 2009, pp. 84-89, 2009. https://doi.org/10.1109/MCOM.2009.4752682

[22] T. C. Yang, "Properties of underwater acoustic communication channels in shallow water", *J. Acoust. Soc. Am.*, vol. 131, no. 1, pp. 129-145, 2012. https://doi.org/10.1121/1.3664053

[23] P. A. van Walree, "Propagation and scattering effects in underwater acoustic communication channels", *IEEE J. Ocean Eng.*, vol. 38, no. 4, pp. 614-631, 2013.

[24] F. John, M. Cimdins, H. Hellbrück, "Underwater ultrasonic multipath diffraction model for short range communication and sensing applications", *IEEE Sensors Journal*, vol. 21, no. 20, pp. 22934-22943, 2021.

[25] J. B. Allen, D. A. Berkley, "Image method for efficiently simulating small-room acoustics". *J. Acoust. Soc. Am.*, vol. 65, no. 4, pp. 943-950, 1979. https://doi.org/10.1121/1.382599

[26] A. Wareing, M. Hodgson, "Beam-tracing model for predicting sound fields in rooms with multilayer bounding surfaces, *J. Acoust. Soc. Am.*, vol. 118, no. 4, pp. 2321-2331, 2005. https://doi.org/10.1121/1.2011152

[27] G. Marbjerg, J. Brunskog, C. H. Jeong, E. Nilsson, "Development and validation of a combined phased acoustical radiosity and image source model for predicting sound fields in rooms". *J. Acoust. Soc. Am.*, vol. 138, no.3, pp. 1457-1468, 2015. https://doi.org/10.1121/1.4928297